International Journal of Advanced Chemistry, 6 (1) (2018) 46-52

International Journal of Advanced Chemistry

Website: www.sciencepubco.com/index.php/IJAC
doi: 10.14419/ijac.v6i1.9048
Research paper

Antibacterial properties of $AgNO_3$-activated carbon composite on Escherichia coli: inhibition action

Nkwaju Yanou Rachel [1], Baçaoui Abdelaziz [2], Ndi Julius Nsami [3], Kouotou Daouda [3]*, Yaacoubi Abdelrani [2], Lourrat Mehdi [2], Lafdi Khalid [4], Ketcha Mbadcam Joseph [3]

[1] *Local Materials Promotion Authority/MIPROMALO, P.O Box: 2396 Yaoundé, Cameroon*
[2] *Department of Chemistry, Faculty of Science Semlalia Marrakech, P.O. Box 2390 Marrakech, University Cadi Ayyad, Morocco*
[3] *Department of Inorganic Chemistry, Faculty of Science, P.O Box 812 Yaoundé, University of Yaoundé I, Cameroon*
[4] *University of Dayton College, 300 College Park, Dayton, OH 45469, USA*
**Corresponding author E-mail: kouotoudaouda@gmail.com*

Abstract

$AgNO_3$- activated carbon composite based palm kernel shell was prepared by hydrothermal carbonization. The concentration of $AgNO_3$, activation temperature and impregnation time were investigated on five responses (iodine number, methylene blue number, BET surface area, micropore volume and total pore volume). The most influential parameters of the preparation process were optimized using the Doehlert optimal design. From the ANOVA, the following optimal conditions of preparation were retained: 0.068 mol/L, 210°C and 3.7 h for $AgNO_3$ concentration, activation temperature and impregnation time respectively. The activated carbon (AC) and the composite (AC-$AgNO_3$) were characterized using Fourier Transform infrared spectroscopy, X-Ray diffraction, Scanning Electron Microscopy coupled to Energy Dispersive X-ray spectroscopy and measurements of the surface area. The XRD pattern and SEM-EDX clearly confirmed the presence of silver in the composite. The experimental parameters of AC- $AgNO_3$ composite were as followed: 708.44 mg/g; 293.09 mg/g; 713.0 m^2/g; 0.49 cm^3/g and 0.76 cm^3/g, for iodine number, methylene blue number, BET surface area, micropore volume and total pore volume of AC- $AgNO_3$ respectively. The antibacterial test carried on Escherichia Coli showed that AC-$AgNO_3$ composite has a high-improved antibacterial property of 99.99% fixation with a dosage of 1500 ppm for 5 hours of contact time.

Keywords: *Activated Carbons; Biomass; Contaminants; Escherichia Coli; Wastewater.*

1. Introduction

Activated Carbon is a black solid substance usually prepared in granular or powder forms [1]. Because of its well-developed porous structures, large active surface area and good mechanical properties, it is currently one of the most effective adsorbent [2]. Activated carbons have been used in industrial wastewater and gas treatment [3], as catalyst support in the catalytic processes and as electrode's materials in electrochemical devices and processes [4]. Significant research has been devoted to the production of activated carbons from lignocellulosic material's wastes [5]. This including, argan shells [6], sugarcane bagasses [7], cherry stones [8], olives wastes cakes [9], date palm tree fronds [10], wood [11], bamboo [12] , palm kernels shell [13, 14], apple pulp [15]. In Cameroun, large quantity of palm kernel shell is generated annually. To reduce these solid wastes and give them an added value, it is better to transform them as activated carbon for the removal of various pollutants. Even if, there are several of activated carbons, the antibacterial activated carbon seems to be interesting in this point of view. Therefore, many authors developed several methods of impregnation of activated carbon by silver followed by a carbonization step at high temperature (up to 600°C). To avoid this energy consumption, the present work proposed to carry out an impregnation with silver on activated carbon at low temperature using a Hydrothermal Carbonization (HTC) techniques. The aforementioned technique is carried out at temperature between 180-300°C with the advantage of obtaining 100% of the impregnated product. Thus, the main objective of this present work is to evaluate the antibacterial properties of the composite activated carbon on Escherichia coli, which is an indicator of fecal contamination. For this purpose, the Doehlert optimal design was used to optimize this process by determining the optimal conditions of impregnation of AC using $AgNO_3$ by HTC technique.

2. Materials and methods

2.1. Raw material

The palm kernel shells were collected in the locality of Bafang in the West region of Cameroon. They were washed intensively with distilled water and sun dried for several days. After that, they were then crushed and sieved to collect particles of sizes ranging between 2- 2.5 mm.

2.2. Activated carbon preparation

30.0 g of sieved palm kernel shell were placed in the furnace at the heating rate of 10 °C/min, from the ambient temperature to 400°C, under a flow of N_2 gas and left for a 2 hours stay at this tempera-

Copyright © 2018 Nkwaju Yanou Rachel et al. This is an open access article distributed under the Creative Commons Attribution License, which permits unrestricted use, distribution, and reproduction in any medium, provided the original work is properly cited.

ture. After which the sample was further heated, under a flow of water steam (0.1mL/min), from 400°C to 850°C and soaked at this final temperature for 6 hours then cooling to room temperature. The activated sample was washed in distilled water, dried, ground, and sieved over a 50µm mesh.

2.2.1. Acid treatment of activated carbon

The activated carbon was carboxylated using concentrated HNO_3 [16]. An amount of 25.0 g of activated carbon was suspended in 500 mL concentrated HNO_3 (1moL/L). The mixture was stirred vigorously for 12 hours at 110°C. The resulting activated carbon was collected by filtration and washed with distilled water to a pH of 7 and dried at 105°C in an oven for 24 hours.

2.2.2. Impregnation of activated carbon by hydrothermal carbonization

A given mass of the functionalized activated carbon was added to an aqueous solution of $AgNO_3$. The mixture was placed in a tubular furnace for Hydrothermal Carbonization, after 1.0 hour, the temperature is set at the desired temperature (180 – 300°C) and desired times (1 – 4 hours) as proposed by the experimental plan. The different samples obtained were washed and dried at 105°C in an oven for further tests.

2.3. Experimental design

Design of experiments consists of a set of mathematical and statistical techniques that can be used to quantify the relationship between output variables (responses) and the input variables [17] in other to determine the optimum operating variables. In this study, the Doehlert experimental design was performed [6]. Three parameters were selected and coded as: X_1 for $AgNO_3$ concentration (0.05-0.1mol/L); X_2 for the impregnation temperature (180-300°C) and X_3 for impregnation time (1-4hours). The performance of the system was estimated by the analysis of five responses which are iodine number (Y_1); methylene blue adsorption (Y_2), BET surface area (Y_3), micropore volume (Y_4) and total pore volume (Y_5). The experimental design matrix of 17 experiments is given in Table 2 above. Each row represents an experimental run, and each column represents the tested variables. The responses are assumed to be affected by three variables and the experimental data were analyzed to fit the following second order polynomial equation:

$$Y = b_0 + b_1 X_1 + b_2 X_2 + b_3 X_3 + b_{11} X_1 X_1 + b_{22} X_2 X_2 + b_3 X_3 X_3 + b_{12} X_1 X_2 + b_{13} X_1 X_3 + b_{23} X_2 X_3 \quad (1)$$

Where, Y is the predicted response, b_0 is the constant coefficient, b_1, b_2; b_3 are the linear coefficients and b_{11}, b_{22}, b_{33} the quadratic coefficients of the X_1, X_2, and X_3 factors respectively. b_{12}, b_{13}, and b_{23}, are the coefficients of the interaction terms X_1X_2, X_1X_3 and X_2X_3 respectively. The data from the Doehlert modeling were treated with the NEMROD software for regression analysis, to fit the equations developed and also to evaluate the statistical significance of the equations obtained.

2.4. Adsorption tests

Two adsorbates were choosen (iodine and methylene blue) for the adsorption tests. The iodine number is determined according to the ASTM D4607-94 Method and was estimated by mixing the activated carbon with 0.02 N of iodine solution shaken for 4.0 hours and then titrated with $Na_2S_2O_3$ solution. For the methylene blue adsorption, 10.0 mg of activated carbon was added to a conical flask containing 100.0 mL of aqueous solution of methylene blue prepared using distilled water in desired concentration. The mixture was stirred for 4.0 hours. The suspension filtered and the concentration of the supernatant determined using an UV-Visible spectrophotometer at a wavelength of 660 nm for methylene blue. The adsorption capacity was calculated using the following formula:

$$Q_{ads} = (C_o - C_e)V/m \quad (2)$$

Where, Q_{ads} (mg/g) is the adsorbed amount, C_o and C_e (mg/L) are the initial and equilibrium concentrations of the iodine or methylene blue solutions respectively. V (L) is the volume of the solution, and m (g) is the mass of the adsorbent used.

2.5. Antibacterial activity

E. coli ATCC25922 was used to study the antibacterial properties of activated carbon and AC-Ag using the plate counting method. The activated carbon and AC- $AgNO_3$ were sterilized in an autoclave at 121°C for 15 min. The amount of materials was adjusted to have concentration from 500 at 1500 ppm and sterilized in an autoclave. A single colony of E. coli was selected and cultured overnight to grow to a concentration of 10^{-6}CFU (Colony forming units)/mL. The sample was placed in distilled water (20.0 mL) containing about 10^{-6}CFU/mL of E.Coli. The mixture was aerobically incubated at 37°C under agitation from 0 to 5.0 hours. At given time period, 1.0 mL of the treated solution was removed and diluted with 100.0 mL of distilled water (this is to adjust the bacterial concentration of the solution to ensure that the bacterial colonies can be easily and correctly counted). 1.0 mL of the dilute solution was transferred onto an agar plate and incubated at 37°C for 24 hours. The number of bacterial colonies on the plate was then counted.

2.6. Characterization

Fourier Transform Infrared (FT-IR) analysis was used to identify the various functional groups on the prepared ACs. Scanning Electron Microscopy (SEM) was used to characterize the surface morphology and Energy Dispersive X-ray (EDX) to determine the chemical composition. The specific surface area, pore volume, total pore volume and pore size distribution of the activated carbon were determined from the Brunauer-Emmett Teller (BET) N_2 adsorption isotherms. The crystalline structure of the materials was examined by X-ray diffraction (XRD) using a copper K□ radiation (λ=1.5406). The content of surface oxygen functional groups was determined by the Boehm method (Nowicky et al. 2015). The point of zero charge was evaluated by the method describes by González-Navarro [18].

3. Results and discussion

3.1. Statistical model analysis

The factorials design, operating conditions and experimental responses are given in Table 1. The experiments at the center point of the complete design matrix were used to determine the experimental error and to verify the reproducibility of experimental results.

The examination of the results given in Table 1 showed that, the quantity of iodine adsorbed (Y_1) varies between 637.64 mg/g and 736.38mg/g. The adsorbed quantities of methylene blue (Y_2) ranged from 175 mg/g to 295 mg/g. The highest quantity of iodine adsorbed (736.38 mg/g) was obtained at [$AgNO_3$] = 0.075 M, at 275°C, and 1.3 hours and that of methylene blue at [$AgNO_3$] = 0,063M, at 257°C; and 3.7 hours. The lowest value was obtained at [$AgNO_3$] = 0.063 M; at 223°C, and at 1.3 hour (experiment 8). For the BET surface area, the highest surface area is obtained for [$AgNO_3$] = 0.075 M; at 205°C and 3.5 hours. Micropore volume and total pore volume, with highest values are obtained for [$AgNO_3$] = 0.063 M; at 257°C, at 3.7 hours. The equations of the polynomial model, as a function of the coded factors, are given as:

$$Y_1 = 716.774 + 3.086X_1 + 10.688X_2 - 0.261X_3 - 10.994X_1^2$$

$$-23.792X_2^2 - 59.568X_3^2 - 7.5X_1X_2 + 3.864X_1X_3 - 113.608X_2X_3 \quad (3)$$

$$Y_2 = 247.084 - 0.724X_1 + 18.104X_2 + 50.512X_3 + 0.741X_1^2 - 43.792X_2^2 + 2.184X_3^2 + 3.297X_1X_2 - 30.376X_1X_3 - 38.180X_2X_3 \quad (4)$$

$$Y_3 = 692.60 + 0.81X_1 + 17.65X_2 + 26.64X_3 - 8.60X_1^2 - 45.60X_2^2 - 47.23X_3^2 - 4.04X_1X_2 - 19.70X_1X_3 - 115.78X_2X_3 \quad (5)$$

$$Y_4 = 0.378 - 0.003X_1 + 0.034X_2 + 0.115X_3 - 0.003X_1^2 - 0.103X_2^2 + 0.006X_3^2 - 0.000X_1X_2 - 0.064X_1X_3 - 0.101X_2X_3 \quad (6)$$

$$Y_5 = 0.674 - 0.003X_1 + 0.034X_2 + 0.091X_3 - 0.001X_1^2 - 0.089X_2^2 + 0.008X_3^2 - 0.006X_1X_2 - 0.072X_1X_3 - 0.087X_2X_3 \quad (7)$$

Table 1: Experimental Design Matrix and Operating Conditions

	Design of experiments			Operating conditions			Experimental responses				
exp	X_1	X_2	X_3	U_1 (mol/L)	U_2 (°C)	U_3 (h)	Y_1 (mg/g)	Y_2 (mg/g)	Y_3 (m^2/g)	Y_4 (cm^3/g)	Y_5 ((cm^3/g)
1	1.0000	0.0000	0.0000	0.100	240	2.5	709.80	249.23	684.81	0.37	0.67
2	-1.0000	0.0000	0.0000	0.050	240	2.5	701.76	246.42	683.19	0.38	0.68
3	0.5000	0.8660	0.0000	0.087	292	2.5	701.58	226.00	670.19	0.33	0.64
4	-0.5000	-0.8660	0.0000	0.063	188	2.5	684.29	205.71	711.50	0.27	0.58
5	0.5000	-0.8660	0.0000	0.087	188	2.5	696.87	196.00	711.51	0.27	0.57
6	-0.5000	0.8660	0.0000	0.063	292	2.5	701.99	230.00	672.88	0.33	0.64
7	0.5000	0.2887	0.8165	0.087	257	3.7	651.68	273.30	646.50	0.43	0.69
8	-0.5000	-0.2887	-0.8165	0.063	223	1.3	640.41	175.00	592.03	0.22	0.53
9	0.5000	-0.2887	-0.8165	0.087	223	1.3	637.64	200.00	610.08	0.27	0.58
10	0.0000	0.5774	-0.8165	0.075	275	1.3	736.38	225.36	688.79	0.32	0.62
11	-0.5000	0.2887	0.8165	0.063	257	3.7	652.47	296.00	662.94	0.48	0.755
12	0.0000	-0.5774	0.8165	0.075	205	3.7	709.00	278.52	712.07	0.47	0.73
13	0.0000	0.0000	0.0000	0.075	240	2.5	716.00	248.15	692.60	0.38	0.67
14	0.0000	0.0000	0.0000	0.075	240	2.5	724.50	246.00	692.60	0.38	0.67
15	0.0000	0.0000	0.0000	0.075	240	2.5	721.59	240.00	693.00	0.38	0.66
16	0.0000	0.0000	0.0000	0.075	240	2.5	720.16	248.07	692.00	0.39	0.67
17	0.0000	0.0000	0.0000	0.075	240	2.5	701.62	253.20	692.6	0.38	0.67

X_1: coded variable of concentration of $AgNO_3$
X_2: coded variable of impregnation Temperature
X_3: coded variable of impregnation time
U_1: natural variable of concentration of $AgNO_3$
U_2: natural variable of impregnation temperature
U_3: natural variable of impregnation time

The positive terms of coefficients of coded values indicate synergistic effects, whereas negative terms indicate antagonistic effect [19]. The quality of the model was evaluated based on the correlation coefficient, R^2 indicating that the variability in the response could be explained by the mathematical model [2]. In this case, the original R^2 and R^2 adjusted are respectively 0.961 and 0.913 for Y_1, 0.986 and 0.969 for Y_2; 0.981 and 0.953 for Y_3, 0.985 and 0.964 for Y_4; 0.987 and 0.968 for Y_5. These R^2 values are relatively high and the difference between the experimental and predicted values is minimal indicating that there is a good agreement between the experimental and predicted responses from the model.
The statistical analysis was carried out using analysis of variance (ANOVA) and Table 2 gives the results for the different responses.

Table 2: Estimated Values of Coefficients for All Response: Y_1, Y_2, Y_3, Y_4 and Y_5

(Y1)

Name	Coefficient	F.Inflation	Standard deviation	t.exp	Signif. %
b0	716.774		4.044	177.23	< 0.01 ***
b1	3.086	1.00	4.522	0.68	52.2
b2	10.688	1.00	4.522	2.36	4.88 *
b3	-0.261	1.00	4.522	-0.06	95.4
b11	-10.994	1.09	7.566	-1.45	18.8
b22	-23.792	1.09	7.567	-3.14	1.61 *
b33	-59.568	1.06	7.102	-8.39	0.0114 ***
b12	-7.500	1.11	10.443	-0.72	50.1
b13	3.864	1.11	11.675	0.33	74.7
b23	-113.608	1.11	11.674	-9.73	< 0.01 ***

(Y2)

Name	Coefficient	F.Inflation	Standard deviation	t. exp	Signif. %
b0	692.60		3.26	212.28	< 0.01 ***
b1	0.81	1.17	4.08	0.20	84.2
b2	17.65	1.06	3.80	4.65	0.382 **
b3	26.64	1.37	4.71	5.66	0.157 **
b11	-8.60	1.09	6.10	-1.41	20.7
b22	-45.60	1.07	6.10	-7.47	0.0446 ***
b33	-47.22	1.32	6.79	-6.95	0.0615 ***
b12	-4.04	1.08	8.42	-0.48	65.1
b13	-19.70	1.55	12.98	-1.52	17.8
b23	-115.78	1.32	10.74	-10.78	< 0.01 ***

(Y3)

Name	Coefficient	F.Inflation	Standard deviation	t.exp	Signif. %
b0	247.084		2.461	100.41	< 0.01 ***
b1	-0.724	1.00	2.751	-0.26	79.5
b2	18.104	1.00	2.751	6.58	0.0408 ***
b3	50.512	1.00	2.751	18.36	< 0.01 ***
b11	0.741	1.09	4.604	0.16	87.1
b22	-43.792	1.09	4.604	-9.51	< 0.01 ***
b33	2.184	1.06	4.321	0.51	63.2
b12	3.297	1.11	6.354	0.52	62.4
b13	-30.376	1.11	7.104	-4.28	0.385 **
b23	-38.180	1.11	7.103	-5.38	0.119 **

(Y4)

Name	Coefficient	F.Inflation	Standard deviation	t. exp	Signif. %
b0	0.378		0.006	62.46	< 0.01 ***
b1	-0.003	1.17	0.008	-0.41	69.4
b2	0.034	1.06	0.007	4.87	0.310 **
b3	0.115	1.37	0.009	13.20	< 0.01 ***
b11	-0.003	1.09	0.011	-0.26	79.4
b22	-0.103	1.07	0.011	-9.10	0.0190 ***
b33	0.006	1.32	0.013	0.46	66.5
b12	-0.000	1.08	0.016	-0.00	100.0
b13	-0.064	1.55	0.024	-2.67	3.64 *
b23	-0.101	1.32	0.020	-5.06	0.261 **

(Y5)

Name	Coefficient	F.Inflation	Standard deviation	t.exp	Signif. %
b0	0.674		0.005	140.67	< 0.01 ***
b1	-0.003	1.17	0.006	-0.52	62.4
b2	0.034	1.06	0.006	6.15	0.107 **
b3	0.091	1.37	0.007	13.13	< 0.01 ***
b11	0.001	1.09	0.009	0.11	91.1
b22	-0.089	1.07	0.009	-9.93	0.0132 ***
b33	-0.008	1.32	0.010	-0.78	47.1
b12	0.006	1.08	0.012	0.47	65.9
b13	-0.072	1.55	0.019	-3.80	0.919 **
b23	-0.087	1.32	0.016	-5.49	0.179 **

*** Very Significant, ** Significant, * Not Significant.

From the ANOVA, the coefficients of impregnation temperature (b_2= 10.688) and the interaction b_{23} (-113. 608) were found to have significant effects on the iodine number. For Y_2 (Methylene

blue), the coefficients of the impregnation temperature (b_2= 18,104), impregnation time (b_3=50,512), and of the interaction term b_{13} (-30.376) and b_{23} (-38.18) indicates that these factors have a significant effect on the quantity of methylene blue adsorbed. For Y_3 (BET surface area), the coefficients b_2 (17.65), b_3 (26.64) and b_{13} (-19.70) have significant effect. For Y_4 (micropore volumes), the coefficients of the impregnation duration (b_3=0.115), temperature b_2 (0.034) and the interactions b_{13} (-0.064) and b_{23} (-0.101) have a significant effect. The coefficients of the impregnation time (b_3=0.091) have also a significant effect as well as the interaction term of impregnation temperature and impregnation time (b_{23} = -0.087) and impregnation time b_{13} (-0.072) for Y_5 (Total pores volume).

From the ANOVA, the coefficients of impregnation temperature (b_2= 10.688) and the interaction b_{23} (-113. 608) were found to have significant effects on the iodine number. For Y_2 (Methylene blue), the coefficients of the impregnation temperature (b_2= 18,104), impregnation time (b_3=50,512), and of the interaction term b_{13} (-30.376) and b_{23} (-38.18) indicates that these factors have a significant effect on the quantity of methylene blue adsorbed. For Y_3 (BET surface area), the coefficients b_2 (17.65), b_3 (26.64) and b_{13} (-19.70) have significant effect. For Y_4 (micropore volumes), the coefficients of the impregnation duration (b_3=0.115), temperature b_2 (0.034) and the interactions b_{13} (-0.064) and b_{23} (-0.101) have a significant effect. The coefficients of the impregnation time (b_3=0.091) have also a significant effect as well as the interaction term of impregnation temperature and impregnation time (b_{23} = -0.087) and impregnation time b_{13} (-0.072) for Y_5 (Total pores volume).

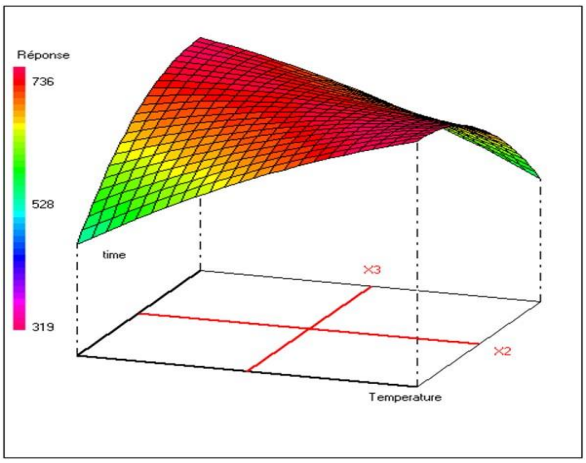

Fig. 1: Variation of the Iodine Adsorption Capacity, I_2/ AC-$AgNO_3$ (Y_1) As a Function of Temperature and Impregnation Time.

3.1.1. Methylene blue (Y2)

The Fig.2 below shows the two and three-dimensional response surface, which were constructed to represent the most important factors on the MB/AC-$AgNO_3$. When the impregnation time is varied from 1.0 to 4.0 hours, the methylene blue adsorption increases from 175 to 295 mg/g, but upon increase of the impregnation temperature, the methylene blue adsorption decreases (Fig. 2a). An increase in impregnation temperature causes, the silver particles to undergo crystallization and a part of the Ag^+ ions are reduced to Ag^0 [20]. As Ag particles are larger in size, they may decrease the adsorption sites on the surfaces of activated carbon [21]. The concentration of $AgNO_3$ therefore has a significant effect on the MB/AC -Ag according the ANOVA. From Fig.2b, the methylene blue adsorption decreases on addition of [$AgNO_3$] from 0.05 to 0.1 M, due to the electrostatic repulsion between Ag^+ and methylene blue resulting in the decrease of available surface exchange sites [22].

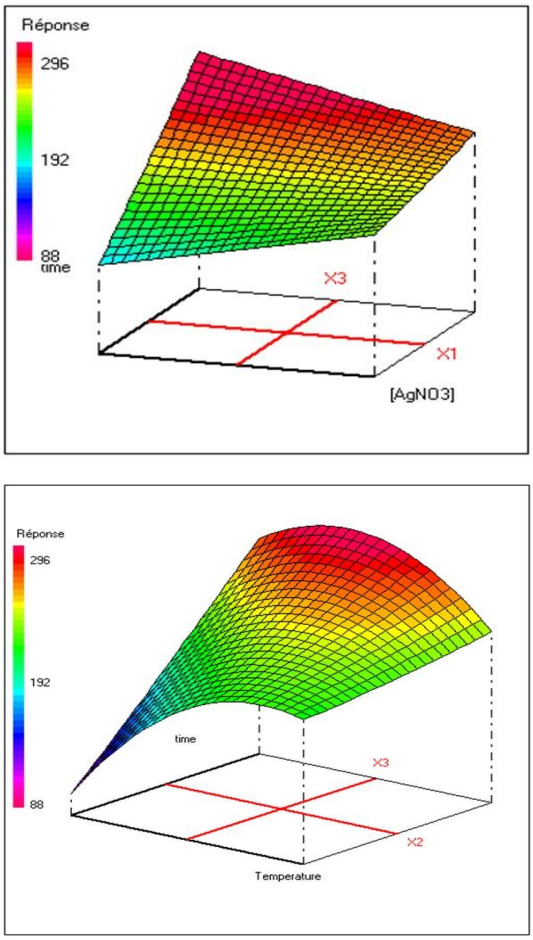

Fig. 2: Variation of the Methylene Blue Adsorption Capacity BM/ AC-$AgNO_3$ (Y_2) as A function of temperature and Time (A) and As A Function of Impregnation Time and [$AgNO_3$] (B).

3.1.2. BET surface area (Y3)

Fig. 3 depicts the variation of BET surface area in the plan temperature – impregnation time, at fixed concentration of silver. An increase in the impregnation duration led to an increase in the BET surface area, due to the development of pores as the time is increased. However, the BET surface area decreases significantly with increase impregnation temperature. The crystallization of Ag at high temperatures causes Ag particle to close the pores and consequently decrease the surface area of activated carbon. As proposed by Asma et al. 2015 this may be due to the destruction of the AC-$AgNO_3$ structure under high heating temperature [23].

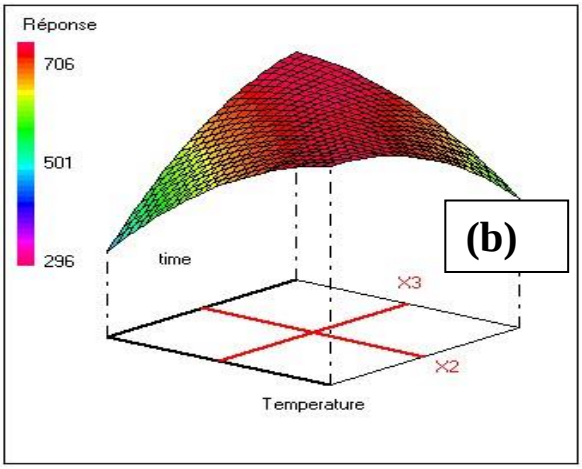

Fig. 3: Variation of the BET Surface Area (S-BET/ AC-$AgNO_3$) As a Function of Temperature and Impregnation Time.

3.1.3. Micropore volume (Y4)

Fig.4 demonstrates that the micropore volume decreases with impregnation concentration of metals. This result indicates that the micropores of the activated carbon were filled or blocked by metals introduced during the process [24]. But this response increased with impregnation time.

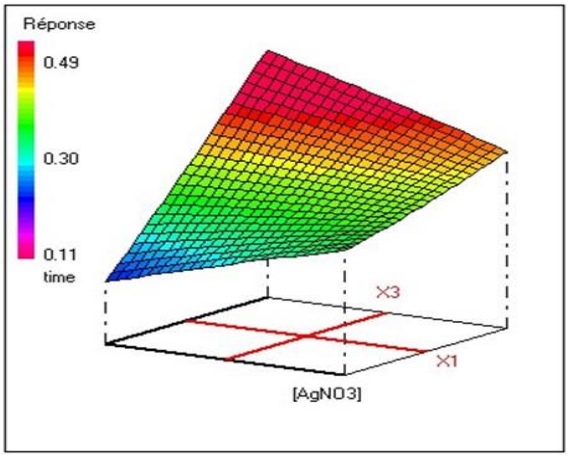

Fig. 4: Variation of the Micropore Volume / AC-$AgNO_3$ as a Function of Temperature and Impregnation Time.

3.1.4. Total pore volume (Y5)

As shown is Fig. 5, the total pore volume increases with an increase in impregnation duration; but decreases significantly with increase in impregnation concentration of $AgNO_3$ and impregnation temperature. The total pore volume (V_{tot}) reduction is indicative of a pore enclosure or structure collapse by further chemical impregnation, thus resulting to a smaller internal volume [25].

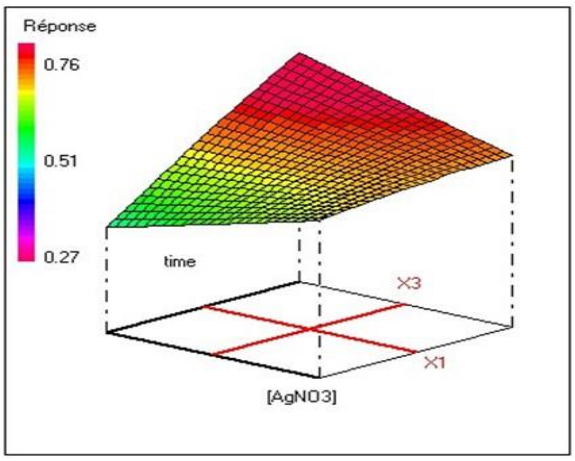

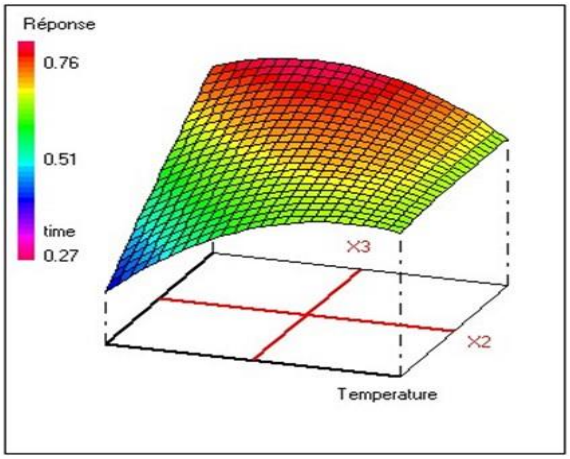

Fig. 5: Variation of Total Pore Volume V_{totale}/ AC-$AgNO_3$ as A Function Of Temperature and Time (A) and As A Function of [$AgNO_3$] and Impregnation Time (B).

3.2. Optimization

The impregnation of activated carbon with silver by hydrothermal carbonization was optimized varying three factors: concentration of $AgNO_3$, impregnation temperature and impregnation duration. The five responses: iodine number, methylene blue, BET surface area, micropore volume and total pore volume were studied. From the optimization studies, It was found that, the impregnation time and temperature have a greater significant effect on all responses. The optimal condition for the impregnation of activated carbon with silver nitrate were obtained at impregnation concentration of $AgNO_3$, of 0.068 mol/L; impregnation temperature of 210°C and impregnation time of 3.7 hours which leads to I_2/AC-$AgNO_3$ of 708.44 mg/g, BM/AC-$AgNO_3$ of 293.09 mg/g, S-BET/AC-$AgNO_3$ of 713.0 m^2/g, Micropores volume/AC-$AgNO_3$ of 0.49 cm^3/g and V_{totale}/AC-$AgNO_3$ of 0.76 cm^3/g.

3.3. Characterization of samples

FTIR spectra were used to identify the functional groups present in AC, AC-HNO_3 and AC-$AgNO_3$. For AC and AC-HNO_3, the intensity of the characteristic peak of 3408.6 cm^{-1} enhanced after oxidative modification which indicates the formation of large number of hydroxyl or phenolic hydroxyl groups on the surface of the oxidized AC [26]. The O–H stretching vibration (3408–3452 cm^{-1}) and C–O stretching vibration (999–1027 cm^{-1}) were more obvious and broader in all samples. The three peaks located at about 1654.6, 1575 and 1562.79 cm^{-1} could be assigned to C=O vibration and an in-plane C=C stretching vibration of aromatic ring, respectively for AC-$AgNO_3$, AC and AC-$AgNO_3$, which support the concept of aromatization activated carbon.

The bands in the range 1000–1500 cm^{-1}, which include the C-O stretching and OH bending vibrations, imply the existence of large numbers of residual hydroxyl groups (OH) and carboxylate groups (COOH) [22]. Acidic and basic surface functionalities were determined by Boehm titration [27]and summarized in Table 3. As it is expected, the total amount of acidic surface groups increased after modification with HNO_3 and $AgNO_3$ respectively.

The XRD patterns for AC and silver modified AC are presented in fig. 7. On both patterns, the broad humps pattern around 24.76° and 44.8° is associated to the amorphous nature of the AC. On the pattern of the modified sample, diffraction peaks at 38.03°, 44.21° and 64.37° (2θ) are observed. Their respective d spacing value of 2.35 Å, 2.04 Å and 1.44 Å, are associated to silver planes (111), (200) and (220) and are evidences for the formation of the AC-Ag composite.

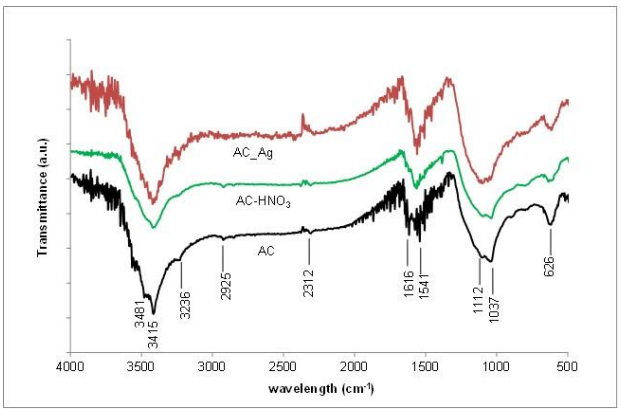

Fig. 6: Infrared Spectra of the Activated Carbon (AC); Nitric Acid Treated AC (AC-HNO_3) and the Silver Nitrate AC Composite (AC-$AgNO_3$).

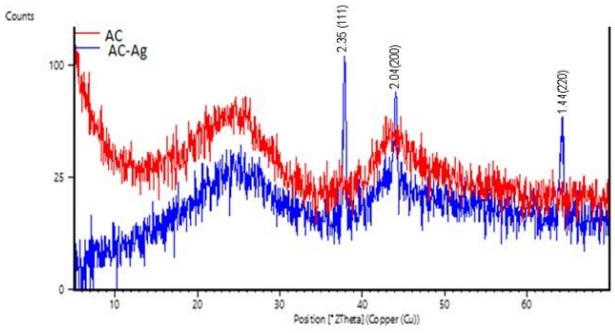

Fig. 7: XRD Patterns of the Activated Carbon (AC) and the Silver Nitrate AC Composite (AC-$AgNO_3$).

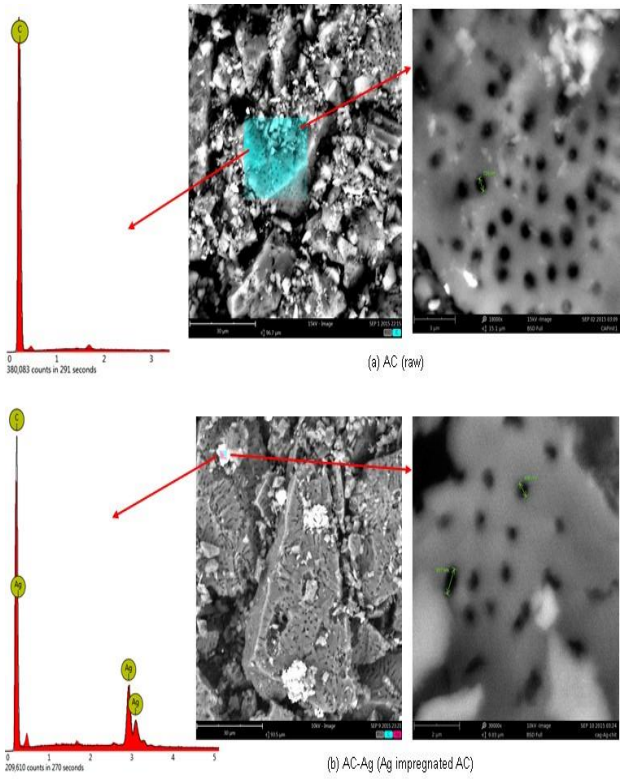

Fig. 8: SEM-EDX of Raw Activated Carbon (A) and Silver Impregnated Activated Carbon (AC-$AgNO_3$) (B).

On the Fig. 8, SEM images and EDX spectra of the raw AC (Fig. 8a) and Ag impregnated AC (Fig. 8b) are presented. The spectrum of the elemental analysis of the colored zone in each image is given (on the left) together with the magnification of the analyzed zone on the right ending of each image. It could be observed on figure 8a, that the AC carbon exhibits and homogenous surface feature chemically characterized by solid carbon. The magnification allowed the visualization of pores of nano size distributed almost homogeneously on the entire surface. After impregnation with silver (Fig. 8b), the elemental analysis indicates the presence of Ag in the material that is in accordance with XRD analysis. The magnification of the local observation shows that, although the surface remained homogeneous, the porosity tends to be reduced, probably due to the occupation of some pore by the Ag particles.

Table 4: Acidic and Basic Groups of the Samples

Samples	Carboxylics group (meq/g)	Lactone groups (meq/g)	Phenolic groups (meqg/g)	Total Acids groups (meqg/g)	Total Basic groups (meqg/g)	pH_{pzc}
PAC	0.5	0	0.25	0.75	1	7.9
AC-HNO_3	0.75	0.25	0.25	1.25	0.5	7.1
AC-Ag	0.75	0.25	0.5	1.5	0.25	6.9

3.4. Antibacterial activity

Antibacterial activities of AC-$AgNO_3$ composites against E.coli were evaluated in comparison to that of AC, and the results are shown on Figures 9. The AC-Ag composite shows a better bactericidal capacity (Fig. 9b), for all dosage, in comparison to the raw AC (Fig. 9a). The anti-bacterial effect is increasing with the dosage and the time. For all dosage, the efficiency of the raw AC is negligible in contrast to the AC-$AgNO_3$ anti-bacterial effect. At a low dosage (500ppm), the AC-Ag composite show good efficiency after 2 hours, after which a decrease effect, associated with the release, by the adsorbent, of the inhibited bacteria that are probably adsorbed on the composite surface. From 1000 ppm, the anti-bacterial effect is increasing up to 5 hours contact time. After 5-hour contact, with a dosage of 1500 ppm, an elimination of approximately 3.4 units log of E. Coli, corresponding to 99.99% reduction of E-coli counts, indicates that the AC-$AgNO_3$ composite is an efficient antibacterial composite. For a contact time of 3 hours and a dosage of 1500 ppm, the raw AC, only induced a 23.68% reduction in E.Coli counts indicating a less efficiency of the raw AC as a bactericide. In addition, when the contact increase a reduction of this efficiency is observed. This reduction is probably due to a release of adsorbed bacteria from the AC surface. These results indicate that the impregnation with silver is very important to obtain a significant bactericidal activity. Hence, the prepared AC-$AgNO_3$ composite is a potential material of interest in water treatment (biological treatment particularly).

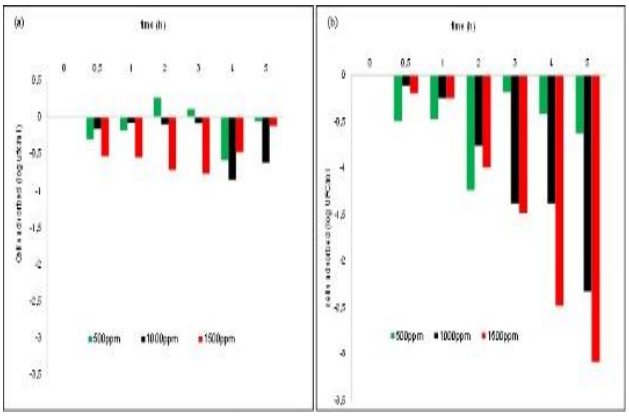

Fig. 9: Elimination of E. Colis by: AC-$Agno_3$ (A) and AC (B).

4. Conclusion

Response Surface Methodology was used to optimize the preparation of AC-$AgNO_3$ by hydrothermal carbonization. A Doehlert design was employed to study the effects of three variables: impregnation concentration of $AgNO_3$, impregnation temperature and impregnation times. It was observed that, the impregnation concentration of silver had a significant effect on the methylene blue adsorption and total pore volume; but had no significant effect on the iodine number, BET surface area or micropore volume. In contrast, the impregnation temperature and impregnation duration have a significant effect on the capacity of all responses. The analyses of the AC-$AgNO_3$ prepared by hydrothermal carbonization using X-ray diffraction and SEM-EDS clearly showed that, the composite material was obtained. Thus, hydrothermal carbonization is a good method to impregnate metal on the surface of activated carbon. The antibacterial test, carried out on the removal of E. Coli in water, showed that the prepared material has a good antibacterial activity. The bactericide effect of the synthesized AC-$AgNO_3$ composite is expected to be of interest in the elimination of bacterial contamination from water and hence limiting the occurrence of waterborne and foodborne diseases.

Acknowledgment

The authors are very greatful to the University of Dayton College, USA for all the analysis done and to those who contributed to the realization of this present work.

References

[1] Sahu JN, Jyotikusum A, Meikap BC (2010), Optimization of production conditions for activated carbons from Tamarind wood by zinc chloride using response surface Methodology. Bioresource. Technology, 101, 1974-1982. https://doi.org/10.1016/j.biortech.2009.10.031.

[2] Sumathi S, Bathia S, Lee KT, Mohammed AR (2009), Optimization of microporous palm shell activated carbon production for flue gas desulphurization: Experimental and statistical studies. Bioresource Technology, 100, 1614-1621. https://doi.org/10.1016/j.biortech.2008.09.020.

[3] Sahin O, Saka C (2013), Preparation and characterization of activated carbon from acorn shell by physical activation with H2O-CO2 in two-step pretreatment. Bioresource Technology, 136, 163-168. https://doi.org/10.1016/j.biortech.2013.02.074.

[4] Walker GM, Weatherley LR (2000), Textile wastewater treatment using granular activated carbon adsorption in fixed beds. Separation Science Technology, 35, 1329-1341. https://doi.org/10.1081/SS-100100227.

[5] Cagnon B, Xavier P, André G, Fritz S, Gerard C (2009), Contributions of hemicellulose, cellulose and lignin to the mass and the porous properties of chars and steam activated carbons from various lignocellulosic precursors. Bioresource Technology, 100, 292-298. https://doi.org/10.1016/j.biortech.2008.06.009.

[6] Ennaciri K, Baçaoui A, Sergent M, Yaacoubi A (2014), Application of fractional factorial and Doehlert designs for optimizing the preparation of activated carbon from argan shells. Chemometrics and Intelligent Laboratory Systems, 139, 48-59. https://doi.org/10.1016/j.chemolab.2014.09.006.

[7] Cronje KJ, Chetty K, Carsky M, Sahu JN, Meikap BC (2011), Optimization of chromium(VI) sorption potential using developped activated carbon from sugarcane bagasse with chemical activation by zinc chloride. Desalinisation. 271, 276-284. https://doi.org/10.1016/j.desal.2011.03.019.

[8] Nowicky P, Kazmierczak J, Pietrzak R (2015), Comparison of physicochemical and sorption properties of activated carbon prepared by physical and chemical activation of cherry stones. Powder Technology, 269, 312-319. https://doi.org/10.1016/j.powtec.2014.09.023.

[9] Baçaoui A, Yaacoubi A, Dahbi A, Bennouna C, Tan Luu RP, Maldonado-Hodar FJ, Rivera-Utrilla J, Moreno-Castilla C (2001), Optimization of conditions for the preparation of activated carbons from olive-waste cakes. Carbon, 39, 425-432 https://doi.org/10.1016/S0008-6223(00)00135-4.

[10] Shoaib M, Al-swaidan HM (2015), Optimization and caractherization of sliced activated carbon prepared from date palm tree fronds by physical activation. Biomass Energy, 73, 124-134. https://doi.org/10.1016/j.biombioe.2014.12.016.

[11] Amaya A, Tancredi N, Silva H, Deiana C (2007), Activated carbon briquettes from biomass materials. Bioresource Technology 98, 1635-1641. https://doi.org/10.1016/j.biortech.2006.05.049.

[12] Gonzalez PJ, Pliego-Cuervo YB (2013), Physicochemical and microtextural characterization of activated carbon produced from water steam activation of three bamboo species. Journal of Analytical and Applied Pyrolysis, 99, 32-39. https://doi.org/10.1016/j.jaap.2012.11.004.

[13] Anirban K, Sen Gupta MAB, Hashim GR (2015), Taguchi optimization approach for production of activated carbon from phosphoric acid impregnated palm kernel shell by microwave heating. Journal of cleaner production, 105, 420-427. https://doi.org/10.1016/j.jclepro.2014.06.093.

[14] Kouotou D, Ngomo Manga H, Baçaoui A, Yaacoubi A, Ketcha Mbadcam J (2014), physicochemical activation of oil palm shells using response surface Methodology: Optimization of activated carbon preparation. International Journal of current Research 5, 431-438.

[15] Suarez-Garcia F, Martinez-Alonso A, Tascon JMD (2002), Pyrolysis of apple pulp: effect of operation conditions and chemical additives. Journal of Analytical and Applied Pyrolysis, 62, 93-109. https://doi.org/10.1016/S0165-2370(00)00216-3.

[16] Amin Yoosefi A, Rong W, Rong X (2013), The effect of regenerable silver nanoparticle/multi-walled Carbon nanotubes coating on the antibacterial performance of hollow fiber membrane. Chemical Engineering Journal, 230, 251-259. https://doi.org/10.1016/j.cej.2013.06.068.

[17] Gandolfi F, Malleret L, Sergent M, Doumenq P (2015), Parameters optimization using experimental design for headspace solid phase micro-extraction analysis of short –chain chlorinated paraffins in waters under the European water framework directives. Journal of Chromatography A, 1406, 59-67. https://doi.org/10.1016/j.chroma.2015.06.030.

[18] Gonzalez-Navarro MF, Goraldo L, Moreno-Pirajan JC (2014), Preparation and characterization of activated carbon for hydrogen storage from waste African oil palm by microwave-induced LIOH basic activation. Journal of Analytical and Applied Pyrolysis, 107, 82-86. https://doi.org/10.1016/j.jaap.2014.02.006.

[19] Tan IAW, Ahmad AL, Hameed BH (2008), Preparation of activated carbon from coconut husk: Optimization study on removal of 2,4,6-trichlorophenol using response surface methodology. Journal of Hazardous Materials, 153, 709–717. https://doi.org/10.1016/j.jhazmat.2007.09.014.

[20] Goscianska J, Nowicki P, Nowak I, Pietrzak R (2012), Thermal analysis of activated carbon modified with silver metavanadate. Thermochimica Acta, 541, 42-48. https://doi.org/10.1016/j.tca.2012.04.026.

[21] Qingchun C, Qingsheng W (2015), Preparation of carbon microspheres decorated with silver nanoparticles and their ability to remove dyes from aqueous solution. Journal of Hazardous Materials, 283, 193-201. https://doi.org/10.1016/j.jhazmat.2014.09.024.

[22] Costas P, Vernon LS (2000), Competitive adsorption between atrazine and methylene blue on activated carbon: the importance of pore size distribution. Carbon, 38, 1423-1436. https://doi.org/10.1016/S0008-6223(99)00261-4.

[23] Asma A, Monia G, Abdelmottalob O (2015), Copper supported on porous activated carbon obtained by wetness impregnation: effects of preparation conditions on the ozonation catalyst's characteristics. Comptes Rendus Chimie, 18, 100-109. https://doi.org/10.1016/j.crci.2014.07.011.

[24] Byung-Joo K, Soo-Jin P (2008), Antibacterial behavior of transition-metals-decorated activated carbon fibers. Journal of Colloid Interface Science, 325, 297-299. https://doi.org/10.1016/j.jcis.2008.05.016.

[25] Roozbeh H, Arami-Niya A, Wan Mohd A, Wan D, Sahu JN (2013), Comparison of oil palm Shell-Based activated carbon produced by microwave and conventional heating methods using zinc chloride activation. Journal of Analytical and Applied Pyrolysis. 104, 176-184. https://doi.org/10.1016/j.jaap.2013.08.006.

[26] Jianghua Q, Guanghui W, Yuncheg B, Danlin Z, Yang C (2015), Effect of oxidative modification of coal tar pitch-based mesoporous activated carbon on the adsorption of benzothiophene and dibenzothiophene. Fuel Process Technology, 129, 85-90. https://doi.org/10.1016/j.fuproc.2014.08.022.

[27] Yavuz G, Zeki A (2014), Nitric acid modification of activated carbon produced from waste tea and adsorption of methylene blue and phenol. Applied Surface Science, 313, 352-359. https://doi.org/10.1016/j.apsusc.2014.05.214.